

Parametric amplification and squeezing with an ac- and dc-voltage biased superconducting junction

Udson C. Mendes,^{1,2,*†} Sébastien Jezouin,¹ Philippe Joyez,² Bertrand Reulet,¹ Alexandre Blais,^{1,3} Fabien Portier,² Christophe Mora,⁴ and Carles Altimiras²

¹ Institut Quantique and Département de Physique, Université de Sherbrooke, Sherbrooke, Quebec J1K 2R1, Canada

² SPEC, CEA, CNRS, Université Paris-Saclay, CEA-Saclay, 91191 Gif-sur-Yvette, France

³ Canadian Institute for Advanced Research, Toronto, Ontario M5G 1Z8, Canada

⁴ Laboratoire Pierre Aigrain, École Normale Supérieure-PSL Research University, CNRS, Université Pierre et Marie Curie-Sorbonne Universités, Université Paris Diderot-Sorbonne Paris Cité, 24 rue Lhomond, 75231 Paris Cedex 05, France



(Received 21 December 2018; published 14 March 2019)

We theoretically investigate a near-quantum-limited parametric amplifier based on the nonlinear dynamics of quasiparticles flowing through a superconductor-insulator-superconductor junction. Photon-assisted tunneling, resulting from the combination of dc- and ac-voltage bias, gives rise to a strong parametric interaction for the electromagnetic modes reflected by the junction coupled to a transmission line. We show phase-sensitive and phase-preserving amplification, together with single- and two-mode squeezing. For an aluminum junction pumped at twice the center frequency, $\omega_0/2\pi = 6$ GHz, we predict narrow-band phase-sensitive amplification of microwaves signals to more than 20 dB, and broadband phase-preserving amplification of 20 dB over a 3-dB bandwidth of 1.2 GHz. We also predict single- and two-mode squeezing reaching more than -12 dB over a 3-dB bandwidth of 5.3-GHz. Moreover, with a simple impedance-matching circuit, we demonstrate a 3-dB bandwidth reaching 4.3 GHz for 20 dB of gain. A key feature of the device is that its performance can be controlled *in situ* with the applied dc- and ac-voltage biases.

DOI: 10.1103/PhysRevApplied.11.034035

I. INTRODUCTION

Many of the advances of quantum computation based on superconducting qubits rely on the ability to readout the qubit state by measuring microwave photons leaking from a superconducting resonator [1]. Because of the development of near-quantum-limited Josephson parametric amplifiers (JPAs) [2–6], high-fidelity single-shot qubit readout is now possible [7,8]. These amplifiers are, moreover, finding use in a wide range of applications, from measurement of quantum features in the radiation emitted by mesoscopic conductors [9–13] to the detection of small ensembles of electronic spins [14], and even to the search for dark matter [15]. JPAs are also versatile sources of single- and two-mode squeezed states [5,16], which have been used to confirm decade-old predictions in quantum optics [17,18] and to improve electron-spin-resonance spectroscopy [14]. Theoretically, squeezed states were proposed as a resource to improve qubit readout and

to perform high-fidelity gates [19–21] or as basis for continuous-variable quantum computing [22,23].

Current JPAs are able to amplify signals to more than 20 dB, and to squeeze vacuum fluctuations by 7 dB (12 dB) in single-mode (two-mode) experiments [5,24]. However, in these devices, the amplification bandwidth is limited to hundreds of megahertz [25–27]. At the price of increasing device-fabrication complexity, much-larger amplification bandwidth, exceeding 3 GHz, has been demonstrated with the recently developed Josephson traveling-wave parametric amplifier [28]. The development of a simpler quantum-limited microwave amplifier, generating far-separated two-mode squeezed states and capable of amplifying signals over gigahertz bandwidths, is still needed to further advance quantum-information-processing science. It would also be an important tool to better characterize the radiation emitted by mesoscopic conductors, for which there is an increasing body of interesting predictions [29–33]. Here we propose a simple broadband parametric amplifier consisting of a single dc- and ac-voltage biased superconductor-insulator-superconductor (SIS) junction. The device can be operated in both phase-sensitive mode and phase-preserving mode and can be used for

*udsonmendes@ufg.br

†Permanent address: Instituto de Física, Universidade Federal de Goiás, CEP 74.690-900, Goiânia, Go, Brazil

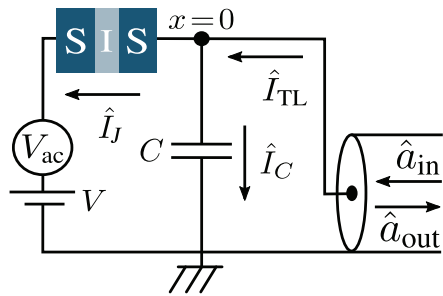


FIG. 1. Electrical scheme of the device: a SIS junction is dc-voltage biased close to the onset of quasiparticle transport $eV_{\text{dc}} \sim 2\Delta$, while it is ac pumped with a single tone $V_{\text{ac}} \cos 2\omega_0 t$. Current conservation at the coupling node ($x = 0$) allows us to relate the transmission-line outgoing field \hat{a}_{out} to its incoming field \hat{a}_{in} and the current flowing through the junction \hat{I}_J .

near-quantum-limited amplification and two-mode squeezing in a bandwidth of a few gigahertz.

The proposed setup, illustrated in Fig. 1, operates as an amplifier in reflection mode. Parametric amplification is possible by taking advantage of the strong nonlinearity of the transport characteristics of the junction. To this end, we consider a dc-voltage bias V_{dc} smaller than twice the superconducting energy gap Δ . At this bias point, the junction behaves as an open circuit and the conduction of quasiparticles is enabled by pumping it with a sinusoidal ac voltage $V_{\text{ac}}(t) = V_{\text{ac}} \cos 2\omega_0 t$, where ω_0 is the center measurement frequency. This voltage combination gives rise to modulations of the admittance of the junction $Y_n(\omega - 2n\omega_0)$, with n the n th sideband of the pump, which generates ac-quasiparticle current at frequency $\omega - 2n\omega_0$. As we show, the most-important terms are $Y_1(\omega - 2\omega_0)$, which is related to the coherent conversion of one quantum of energy $2\hbar\omega_0$ from the pump to two photons of frequencies $\omega \approx \omega_0$, and $Y_0(\omega)$, which is related to single-photon coherent (imaginary part) and dissipative (real part) response due to the tunneling of quasiparticles. By appropriately choosing the dc voltage to be less than twice the superconducting gap, we demonstrate that it is possible to make $|Y_1(\omega - 2\omega_0)|$ large enough while keeping $\text{Re}Y_0(\omega)$ close to zero to generate parametric amplification with near-quantum-limited noise and squeezing. Furthermore, $\text{Im}Y_0(\omega)$ gives rise to a large frequency-dependent impedance mismatch that limits the gain and squeezing bandwidths. Fortunately, as we show in Sec. III C, this frequency-dependent impedance mismatch can be handled with an impedance-matching scheme.

It is surprising that even though SIS junctions are routinely used as high-frequency microwave quantum-limited mixers [34,35], using a very similar principle, their operation as parametric amplifiers have been mostly disregarded [36,37]. Here we use the input-output formalism [38] together with photon-assisted tunneling theory [39]

to compute the parametric amplification and squeezing properties of an ac- and dc-voltage biased SIS junction [40]. The resulting Heisenberg-Langevin equations [41] are numerically solved, allowing us to explore parametric amplification far from the small detuning limit considered previously [36,37]. For an aluminum junction ($\Delta = 180 \mu\text{eV} \sim h \times 43.5 \text{ GHz}$) pumped at $2\omega_0 = 2\pi \times 12 \text{ GHz}$ and operated at temperatures $T \ll \Delta/k_B$, with k_B the Boltzmann constant, we find that when it is operated in experimentally relevant conditions, the device can produce more than 20 dB of phase-preserving and phase-sensitive gain, and approximately 13 dB of single- and two-mode squeezing. In the phase-preserving mode, the 3-dB gain bandwidth exceeds 1.2 GHz and, therefore, it is twice as large as the bandwidth of the broadband-impedance-engineered JPA [27]. Moreover, the 3-dB gain and squeezing bandwidths can be increased to 4.3 GHz with impedance-matching schemes to compensate both the geometrical capacitance C and the dynamical susceptance $\text{Im}Y_0$ of the junction [27].

This article is organized as follows: In Sec. II we describe the input-output formalism used to characterize the device. Section III A presents results for an ideal SIS junction for which the transport response rises steeply at $eV_{\text{dc}} = 2\Delta - n\hbar\omega_0$. The effects of the low-frequency noise, which captures most of the nonideal effects, on the amplifier is described in Sec. III B. An approach to improve further the performance of the amplifier relying on impedance engineering is presented in Sec. III C. Final remarks are presented in Sec. IV.

II. MODEL

We consider a SIS junction in parallel with its capacitance and connected to a transmission line (TL), see Fig. 1. The total Hamiltonian of the device is $\hat{H} = \hat{H}_{\text{qp}} + \hat{H}_{\text{ee}} + \hat{H}_{\text{tun}}$, where

$$\hat{H}_{\text{qp}} = \sum_l \epsilon_l \hat{c}_l^\dagger \hat{c}_l + \sum_r \epsilon_r \hat{c}_r^\dagger \hat{c}_r \quad (1)$$

describes the quasiparticles in the left (l) and right (r) superconductors forming the junction. In this expression, \hat{c}_l (\hat{c}_r) annihilates a quasiparticle of energy ϵ_l (ϵ_r) in the left (right) superconductor. The Hamiltonian describes the dynamics of quasiparticles. However, Cooper pairs are also present and interact with the electromagnetic field. Since we are interested in signals of frequency $\omega_0 \ll \Delta/\hbar$ amplified or squeezed by operating the junction close to the onset of quasiparticle transport $eV_{\text{dc}} \approx 2\Delta$, we ignore the effects from the tunneling of Cooper pairs whose Josephson frequency is approximately $4\Delta/\hbar \gg 2\omega_0$. Experimentally, the effects of Cooper pairs can be further suppressed by the passing of one flux quantum within a SIS junction

[40]. This suppression can be done either by fabrication of the junction in a superconducting-quantum-interference-device geometry or by application of an in-plane magnetic field to the junction [35].

The Hamiltonian of the electromagnetic environment, which includes the TL and the capacitor C of the junction, is

$$\hat{H}_{\text{ee}} = \frac{\hat{Q}^2(x=0)}{2C} + \int_0^\infty dx \left[\frac{1}{2L_0} \left(\frac{\partial \hat{\Phi}(x)}{\partial x} \right)^2 + \frac{\hat{Q}^2(x)}{2C_0} \right]. \quad (2)$$

The first and second terms account for the charging energy of the capacitor and the TL dynamics. The charge $\hat{Q}(x)$ and flux $\hat{\Phi}(x)$ operators obey $[\hat{\Phi}(x), \hat{Q}(x')] = i\hbar\delta(x - x')$. The TL characteristic impedance $Z_0 = \sqrt{L_0/C_0}$ is defined in terms of its inductance L_0 and capacitance C_0 per unit length. Finally, the last term in the total Hamiltonian is the tunneling of quasiparticles dressed by the environment and it takes the form [42]

$$\hat{H}_{\text{tun}} = \hat{T}(t) \exp[ie\hat{\Phi}(t)/\hbar] + \text{H.c.}, \quad (3)$$

where $\hat{T}(t) = \sum_{l,r} t_{lr} \hat{c}_l^\dagger \hat{c}_r \exp\{i[eV_{\text{dc}}t/\hbar + \varphi_{\text{ac}}(t)]\}$ is the tunneling operator transferring a quasiparticle from the right to the left side of the junction with tunneling probability amplitude $t_{lr} \equiv t_{rl}$. The phase $\varphi_{\text{ac}}(t) = (eV_{\text{ac}}/2\hbar\omega_0) \sin 2\omega_0 t$ takes into account the ac voltage, and $\hat{\Phi}(t) \equiv \hat{\Phi}(t, x=0)$ is the TL flux at the position of the junction.

In the interaction picture with respect to \hat{H}_{tun} , this TL flux is written in terms of the incoming $\hat{a}_{\text{in}}[\omega]$ and outgoing $\hat{a}_{\text{out}}[\omega]$ fields as [38]

$$\hat{\Phi}(t, x) = \sqrt{\frac{\hbar Z_0}{4\pi}} \int_0^\infty \frac{d\omega}{\sqrt{\omega}} (\hat{a}_{\text{in}}[\omega] e^{-i(\omega t + k_\omega x)} + \hat{a}_{\text{out}}[\omega] e^{-i(\omega t - k_\omega x)} + \text{H.c.}), \quad (4)$$

where $k_\omega = \omega\sqrt{L_0 C_0}$ is the wave number. The incoming (outgoing) field obeys the commutation relation $[\hat{a}_{\text{in}}[\omega], \hat{a}_{\text{in}}^\dagger[\omega']] = \delta(\omega - \omega') \{[\hat{a}_{\text{out}}[\omega], \hat{a}_{\text{out}}^\dagger[\omega']] = \delta(\omega - \omega')\}$.

To characterize the radiation emitted by the junction, we use the input-output formalism adapted to circuits coupled to quantum conductors [31,43,44]. To obtain the input-output boundary condition, the first step is to derive the Heisenberg equations of motion for both TL charge and flux at the position of the junction ($x = 0$). The resulting equations are combined to express current conservation

$$\ddot{C\hat{\Phi}}(t, x=0) - \frac{1}{L_0} \frac{\partial \hat{\Phi}(t, x)}{\partial x} \Big|_{x=0} = \hat{I}_J(t), \quad (5)$$

which connects the outgoing field to the incoming field and the current of the junction $\hat{I}_J(t)$. Using Eq. (4), we can express Eq. (5) as an input-output relation:

$$\hat{a}_{\text{out}}[\omega] = \frac{1 + iZ_0C\omega}{1 - iZ_0C\omega} \hat{a}_{\text{in}}[\omega] + i\sqrt{\frac{Z_0}{\pi\hbar\omega}} \frac{\hat{I}_J[\omega]}{1 - iZ_0C\omega}, \quad (6)$$

where $\hat{I}_J[\omega]$ is the Fourier transform of $\hat{I}_J(t)$. The first term describes the phase shift due to the reflection of the input field by the capacitor. The last term characterizes the radiation emitted by the junction and it gives rise to both current fluctuations and a deterministic response to the applied voltages [43,44].

The current $\hat{I}_J[\omega]$ depends not only on the dc and ac voltages but also on the TL voltage, $\hat{V}_{\text{TL}}(t) = \dot{\hat{\Phi}}(t)$, implying that $\hat{I}_J[\omega]$ and $\hat{a}_{\text{in}}[\omega]$ do not commute. To circumvent the noncommutation between $\hat{I}_J[\omega]$ and $\hat{a}_{\text{in}}[\omega]$, we take advantage of the weak TL-junction coupling $\sqrt{\pi Z_0/R_K} \ll 1$ (for a typical $Z_0 = 50 \Omega$ TL impedance [9,10], with $R_K \simeq 25.8 \text{ k}\Omega$ the quantum of resistance) and compute $\hat{I}_J[\omega]$ to second order in the TL-junction coupling [32,43]. In the time domain and for weak coupling to the environment, the current operator, in the Heisenberg picture, takes the form

$$\hat{I}_J(t) = \hat{I}_{\text{qp}}(t) + \frac{e^2}{\hbar^2} \hat{H}_{\text{qp}}^{\text{tun}}(t) \hat{\Phi}(t), \quad (7)$$

where $\hat{I}_{\text{qp}}(t) = i(e/\hbar)[\hat{T}^\dagger(t) - \text{H.c.}]$ and $\hat{H}_{\text{qp}}^{\text{tun}}(t) = \hat{T}(t) + \text{H.c.}$ are, respectively, the quasiparticle current and tunneling operators in the absence of TL voltage. The final step is to time-evolve $\hat{I}_J(t)$. With use of linear-response theory, the quasiparticle operators are time-evolved, in the interaction picture, with the interaction Hamiltonian $H_{\text{int}}(t) = -\hat{I}_{\text{qp}}^i(t) \hat{\Phi}^i(t)$, where superscript i means the operator in the interaction picture. Once more, we take advantage of the weak TL-junction coupling and the short interaction time between the quasiparticles and photons to expand the time-evolution operator to first order in $\hat{\Phi}^i(t)$ to obtain

$$\begin{aligned} \hat{I}_J(t) &= \hat{I}_{\text{qp}}^i(t) + \frac{e^2}{\hbar^2} \hat{H}_{\text{qp}}^{\text{tun}(i)}(t) \hat{\Phi}^i(t) \\ &\quad - \frac{i}{\hbar} \int_{-\infty}^t \hat{\Phi}^i(t') [\hat{I}_{\text{qp}}^i(t'), \hat{I}_{\text{qp}}^i(t)] dt'. \end{aligned} \quad (8)$$

The first term is the current operator due to quasiparticle tunneling and it depends on the ac- and dc-voltage biases, while the last two terms describe modifications of the current fluctuations due to the TL field. In the weak-interaction limit considered here, we average over the quasiparticle operators in the terms proportional to $\hat{\Phi}^i(t)$;

that is,

$$\hat{I}_J(t) = \hat{I}_{qp}^i(t) + \frac{e^2}{\hbar^2} \langle \hat{H}_{qp}^{\text{tun}(i)}(t) \rangle \hat{\Phi}^i(t) - \frac{i}{\hbar} \int_{-\infty}^t \hat{\Phi}^i(t') \langle [\hat{I}_{qp}^i(t'), \hat{I}_{qp}^i(t)] \rangle dt'. \quad (9)$$

This approximation is equivalent to the Born-Markov approximation [32,43]. Under these approximations, the current operator is written in frequency space as

$$\hat{I}_J[\omega] = \hat{I}_{qp}^i[\omega] - \sum_{n=-\infty}^{\infty} Y_n(\omega - 2n\omega_0) \hat{V}_{\text{TL}}^i[\omega - 2n\omega_0], \quad (10)$$

where $\hat{I}_{qp}^i[\omega]$ and $\hat{V}_{\text{TL}}^i[\omega]$ are the Fourier transforms [45] of $\hat{I}_{qp}^i(t)$ and $\hat{V}_{\text{TL}}^i(t)$, respectively. The generalized admittance

$$Y_n(\omega) = \frac{i}{\hbar} \int \frac{d\omega_1}{2\pi} \frac{S_n(\omega_1) - S_n(2n\omega_0 - \omega_1)}{(\omega_1 + \omega + i0^+)(\omega_1 + i0^+)} \quad (11)$$

relates the current response at frequency ω to the TL-voltage dynamics at frequency $\omega - 2n\omega_0$ [44]. The admittance is defined in terms of the photon-assisted current-current correlator $\langle \hat{I}_{qp}^i(\omega) \hat{I}_{qp}^i(\omega') \rangle = 2\pi \sum_n S_n(\omega) \delta(\omega + \omega' - 2n\omega_0)$, where

$$S_n(\omega) = \frac{1}{2} \sum_{n_1=-\infty}^{\infty} J_{n_1}(\rho) [J_{n_1+n}(\rho) S_{\text{eq}}(\hbar\omega + eV_{\text{dc}} + 2n_1\hbar\omega_0) + J_{n_1-n}(\rho) S_{\text{eq}}(\hbar\omega - eV_{\text{dc}} - 2n_1\hbar\omega_0)] \quad (12)$$

is nonsymmetrized photon-assisted current noise [32,43,44]. It is defined in terms of the Bessel function $J_n(\rho = eV_{\text{ac}}/2\hbar\omega_0)$ and the equilibrium current noise $S_{\text{eq}}(\omega) = 2e[\hat{I}_{qp}^i[\omega]]/[1 - \exp(-\hbar\omega/k_B T)]$ [46].

Equation (10) describes the linear response of the junction due to TL-voltage fluctuations. In the absence of ac voltage, the linear response is strictly local in frequency with $Y_{n \neq 0}(\omega - 2n\omega_0) = 0$. On the other hand, the addition of the ac bias leads to $Y_{n \neq 0}(\omega - 2n\omega_0) \neq 0$ due to TL-voltage fluctuations at frequencies of the pump sidebands $2n\omega_0$. It is important to mention that $Y_{n \neq 0}(\omega - 2n\omega_0)$ is nonzero only for nonlinear junctions [44]. Consequently, in this device, parametric interaction is due to the combination of photon-assisted transport and nonlinearity. For instance, the nonlinearity converts a single pump photon of frequency $2\omega_0$ into two photons of frequency ω_0 [47]. In the SIS amplifier, this process is characterized by $Y_1(\omega - 2\omega_0)$ and allows parametric amplification and squeezing [32]. As will be clear from Eq. (15), parametric amplification arises when $|Y_1(-\omega_0)| \approx |Z_0^{-1} + Y_0(\omega_0) - iC\omega_0|$. Figure 2 illustrates the dc-voltage dependence of $Y_1(-\omega_0)$

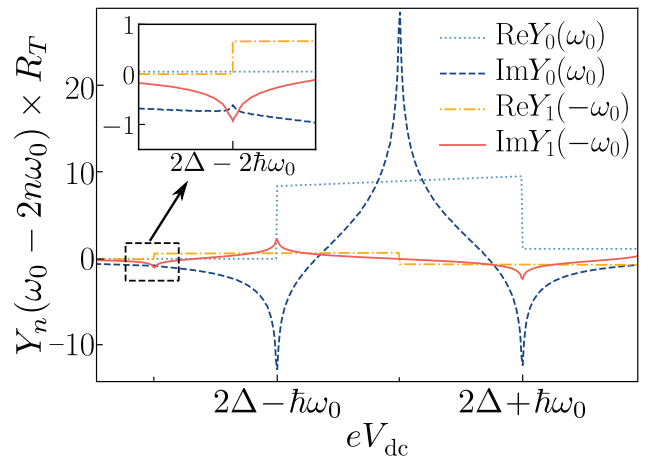


FIG. 2. Nonlinear admittance as a function of the dc voltage for an aluminum junction ($\Delta = 180 \mu\text{eV} \sim h \times 43.5 \text{ GHz}$, $eV_{\text{ac}} = 0.155 \times 2\hbar\omega_0$, and $\omega = \omega_0 = 2\pi \times 6 \text{ GHz}$). On the one hand, as shown in Sec. II, $\text{Im}Y_0(\omega_0)$ and $\text{Re}Y_0(\omega_0)$ give rise, respectively, to coherent and dissipative absorption and emission of single photons. However, the pumping gives rise to a parametric interaction characterized by a sizable nonlinear admittance $Y_1(-\omega_0)$. For dc voltages $eV_{\text{dc}} \sim 2(\Delta - \hbar\omega_0)$ and with the appropriate ac-voltage amplitude, the nonlinear susceptibility $Y_1(-\omega_0)$ dominates over the single-photon coherent and dissipative response $Y_0(\omega)$, giving rise to parametric amplification and squeezing (see the inset).

and $Y_0(\omega_0)$ for a weak pump amplitude $eV_{\text{ac}} = 0.155 \times 2\hbar\omega_0$. From the above criteria, parametric amplification and squeezing occurs for $eV_{\text{dc}} \approx 2\Delta - 2\hbar\omega_0$ (see the inset in Fig. 2). At this dc voltage, single-photon dissipation $\text{Re}Y_0(\omega_0)$ is approximately zero, which is a necessary condition to reach near-quantum-limited noise and a large degree of squeezing by virtue of the fluctuation-dissipation theorem. Unsurprisingly, this dc voltage is also the optimal operational point of SIS mixers [40]. In Fig. 2, the admittance present discontinuities for dc voltages $eV_{\text{dc}} = 2\Delta - n\hbar\omega_0$. These discontinuities are a characteristic of photon-assisted transport and nonlinearity. The real parts exhibit jumps that are replicas of the SIS $I-V$ curve, while the imaginary parts exhibit logarithmic singularities. In practice, these discontinuities are rounded by experimental noise, a finite Dynes parameter [48], finite temperature, and, in our simulations, numerical precision. Finally, it is important to emphasize that $\hat{I}_{qp}^i[\omega]$ and $Y_n(\omega - 2n\omega_0)$ depend only on the quasiparticle dynamics determined by $H_{qp} + H_{qp}^{\text{tun}}(t)$ and on the intrinsic characteristics of the junction (e.g., the superconducting gap Δ and normal-state resistance R_T).

As mentioned above, parametric interaction emerges from two-photon processes characterized by $Y_1(\omega - 2\omega_0)$, while single-photon processes are characterized by $Y_0(\omega)$. The other nonlocal frequency contributions, from the second term in Eq. (10), give rise to conversion processes

where photons of frequency $|\omega| > 2\omega_0$ are up- or down-converted to ω . As these contributions are detrimental to amplification and squeezing, we consider that an on-chip low-pass filter is used to filter all frequencies above $2\omega_0$. As a consequence, we can safely ignore all the contributions to the current operator originating from $n \neq 0, 1$ in the sum over n in Eq. (10), which takes the form

$$\hat{I}_J[\omega] = \hat{I}_{\text{qp}}^i[\omega] - Y_0(\omega)\hat{V}_{\text{TL}}^i[\omega] - Y_1(\omega - 2\omega_0)\hat{V}_{\text{TL}}^i[\omega - 2\omega_0]. \quad (13)$$

In addition to the low-pass filter, the $R_T C$ time of the junction acts as a high-frequency cutoff. For the results presented in the next section, we take $\omega_{RC} = 1/R_T C = 2\pi \times 30$ GHz as a fixed parameter of the junction, which is obtained for a normal-state resistance $R_T = 50 \Omega$ and $C = 100 \text{ fF}$.

Within these approximations, the expression for the outgoing field in terms of the incoming field and the quasiparticle current operators is obtained by substitution of Eq. (13) into Eq. (6). After simple algebraic manipulation, the outgoing field is

$$\hat{a}_{\text{out}}[\omega_0 + \omega'] = r(\omega')\hat{a}_{\text{in}}[\omega_0 + \omega'] + \gamma(\omega')\hat{a}_{\text{in}}^\dagger[\omega_0 - \omega'] + \alpha(\omega')\hat{I}_{\text{qp}}[\omega_0 + \omega'] + \beta(\omega')\hat{I}_{\text{qp}}^\dagger[\omega' - \omega_0], \quad (14)$$

where $\omega' = \omega - \omega_0$ is the frequency detuning and the reflection coefficient

$$r(\omega') = \frac{[Z_0^{-1} - Y_J(\omega_s)][Z_0^{-1} + Y_J^*(\omega_i)] + \Gamma(\omega)}{[Z_0^{-1} + Y_J(\omega_s)][Z_0^{-1} + Y_J^*(\omega_i)] - \Gamma(\omega')}, \quad (15)$$

where we defined $Y_J(\omega) = Y_0(\omega) - iC\omega$, $\omega_s = \omega_0 + \omega'$ and $\omega_i = \omega_0 - \omega'$, and $\Gamma(\omega') = Y_1(\omega' - \omega_0)Y_1^*(-\omega' - \omega_0)$. Here, terms proportional to Z_0^{-1} and $\text{Re } Y_0(\omega)$ are the internal TL decay rates at which the junction absorbs and emits photons, respectively. The terms proportional to C and $\text{Im } Y_0(\omega)$ are related to the geometrical capacitance and dynamical susceptance of the junction. In the second term in Eq. (14), we introduced $\gamma(\omega') = 2\sqrt{\omega_i/\omega_s}Y_1(\omega' - \omega_0)/Z_0\Delta\omega'$, with $\Delta\omega' = [Z_0^{-1} + Y_J(\omega_s)][Z_0^{-1} + Y_J^*(\omega_i)] - \Gamma(\omega')$. As expected, the Fourier coefficient of $\hat{a}_{\text{in}}^\dagger$ is proportional to Y_1 . Moreover, the coefficients of $\hat{I}_{\text{qp}}[\omega' \pm \omega_0]$ are $\alpha(\omega') = \mu_{\omega_s}[Z_0^{-1} + Y_J^*(\omega_i)]$ and $\beta(\omega') = \mu_{\omega_s}^*Y_1(\omega' - \omega_0)$, with $\mu_{\omega_s} = i/\Delta\omega'\sqrt{\pi Z_0\hbar\omega_s}$.

Equation (14) is a central result of this paper and shows that the dc- and ac-voltage biased SIS junction acts as an amplifier operating in reflection mode. More specifically, for a fixed frequency detuning $\omega' \neq 0$, the operators $\hat{a}_{\text{in}}[\omega' + \omega_0]$ and $\hat{a}_{\text{in}}[\omega_0 - \omega']$ commute and can be seen as the input-signal and the idler-mode operators of a phase-preserving amplifier [47,49]. In this mode, the gain is

given simply by $G(\omega') = |\hat{a}_{\text{out}}[\omega']|^2$ and the last two terms in Eq. (14) correspond to added noise beyond the quantum limit $\mathcal{A}_q(\omega') = [1 - 1/G(\omega')]/2$. To characterize the effects of quasiparticle tunneling on the performance of the amplifier, we compute the added noise using the relation $\langle |\hat{a}_{\text{out}}[\omega]| \rangle = G(\omega)(\mathcal{A}(\omega) + \langle |\hat{a}_{\text{in}}[\omega]| \rangle)$ [24,49], with $\langle |\hat{O}| \rangle = \langle \hat{O}^\dagger \hat{O} + \hat{O}\hat{O}^\dagger \rangle/2$ and the added noise

$$\begin{aligned} \mathcal{A}(\omega') = \mathcal{A}_q(\omega') + \frac{2\pi}{G(\omega')} \{ & |\alpha(\omega')|^2 S_0(\omega_s) \\ & + |\beta(\omega')|^2 S_0(-\omega_i) - 2\text{Re}[\alpha(\omega')\beta^*(\omega')]S_1(\omega_s) \}. \end{aligned} \quad (16)$$

The terms proportional to $S_0(\omega_s)$, $S_0(-\omega_i)$, and $S_1(\omega_s)$ are noise generated by the tunneling of quasiparticles, and they originate from absorption and emission of one quantum and two quanta of energy $\hbar\omega_0$ by the junction. As expected, the quasiparticle noise $S_n(\omega)$ increases the added noise of the amplifier. Thus, to mitigate the effects of the quasiparticle noise, the operational voltages of the device are such that $S_0(\omega_s)$, $S_0(-\omega_i)$ and $S_1(\omega_s)$ are as small as possible. To characterize the deviation of the quantum limit, we define the quantum efficiency of the parametric amplifier as $\xi = \mathcal{A}_q(\omega)/\mathcal{A}(\omega)$. For an ideal phase-preserving amplifier $\xi = 1$ and in the presence of quasiparticle noise $\xi < 1$.

For $\omega' = 0$, $\hat{a}_{\text{in}}[\omega_0]$ and $\hat{a}_{\text{in}}^\dagger[\omega_0]$ do not commute, and the first two terms in Eq. (14) rather characterize an ideal phase-sensitive amplifier [47,49]. In this operational mode, the gain $G(0)$ is defined as a combination of $r(0)$, $\gamma(0)$, and the phases of the input and output fields [24]. The added noise is given by a linear combination of the two last terms in Eq. (14) and it also depends on the input- and output-field phases [24].

To better characterize the radiation emitted by the SIS amplifier, we compute the output power spectrum $S_\theta(\omega)$, defined in terms of $\langle \Delta\hat{X}_\theta[\omega]\Delta\hat{X}_\theta[\omega_1] \rangle = S_\theta(\omega)\delta(\omega + \omega_1)$, where $\hat{X}_\theta[\omega'] = e^{-i\theta}\hat{a}_{\text{out}}[\omega' + \omega_0] + e^{i\theta}\hat{a}_{\text{out}}^\dagger[\omega_0 - \omega']$ is the output-field quadrature with fluctuations $\Delta\hat{X}_\theta[\omega] = \hat{X}_\theta[\omega] - \langle \hat{X}_\theta[\omega] \rangle$ and θ is the phase of the output field. Similarly to amplification, the emitted radiation can be characterized by a single-mode $S_\theta(\omega' = 0) < 1$ or a two-mode $S_\theta(\omega' \neq 0) < 1$ squeezed state.

III. RESULTS

We first present results for an ideal SIS junction, with transport response rising steeply for voltages $eV_{dc} = 2\Delta - n\hbar\omega_0$ as illustrated in Fig. 2(b). We then investigate how gain and squeezing properties are affected by low-frequency noise, which smooth out the transport response of the junction and, consequently, diminish the strength of the parametric interaction. Lastly, an impedance-matching scheme is presented. This scheme is used to match both

the geometrical capacitance (C) and the dynamical susceptance [$\text{Im}Y_0(\omega)$] of the junction, thus leading to much larger bandwidths.

A. Ideal SIS junction

Before considering the general frequency-dependent amplification and squeezing, we present results for zero frequency detuning ($\omega' = 0$). First, we investigate the effect of the strength of nonlinearities on the phase-sensitive mode. Figures 3(a) and 3(b) illustrate, respectively, the phase-sensitive gain and single-mode squeezing as a function of $\Delta/\hbar\omega_0$ when V_{ac} is optimized to maximize single-mode squeezing for $eV_{\text{dc}} = 2\Delta - 1.999\hbar\omega_0$ (see the horizontal solid line in Fig. 4). This dc voltage is in the vicinity of the logarithmic singularity shown in the inset in Fig. 2; its choice is explained in Fig. 4. In Fig. 3, Δ varies while $\omega_0/2\pi$ is kept fixed at 6 GHz. Already at small $\Delta/\hbar\omega_0 \approx 2$ we observe more than 10 dB of amplification and approximately -8 dB of squeezing. As $\Delta/\hbar\omega_0$ increases, the strength of the nonlinearities giving rise to parametric interaction increases, thus enhancing gain and squeezing as illustrated in Fig. 3. Thus, increasing Δ leads to an increase of the parametric interaction strength proportional to $Y_1(\omega)$. For $\Delta/\hbar\omega_0 = 20$, amplification and squeezing reach approximately 27 dB and -13.5 dB, respectively. Here the filled area corresponds to $\omega_0/2\pi$ in the 4–10-GHz range for an aluminum junction with $\Delta/h \approx 43.5$ GHz. A larger value of Δ can be obtained by reduction of the thickness of the aluminum layer [50]

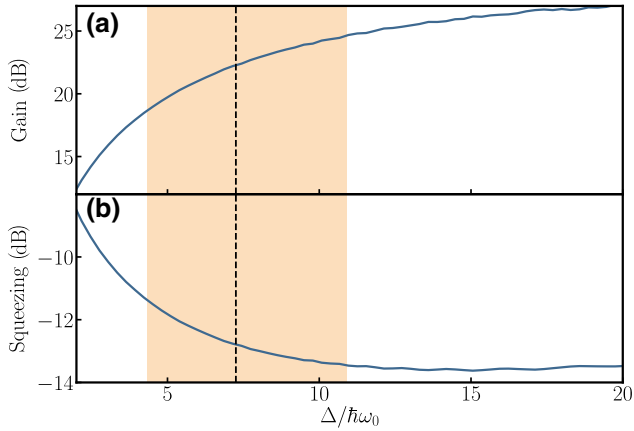


FIG. 3. (a) Phase-sensitive gain and (b) single-mode squeezing as a function of $\Delta/\hbar\omega_0$ for $\omega_0/2\pi = 6$ GHz. The filled area corresponds to values for an aluminum superconducting junction ($\Delta = 180$ μ eV) for $\omega_0/2\pi$ in the 4–10-GHz range and the dashed line marks $\omega_0/2\pi = 6$ GHz used to investigate the frequency-dependent gain and squeezing. For each value of $\Delta/\hbar\omega_0$, the dc voltage is fixed to $eV_{\text{dc}} = 2\Delta - 1.999\hbar\omega_0$ and the ac voltage is optimized to maximize squeezing. The optimal ac-voltage amplitude diminishes as $\Delta/\hbar\omega_0$ increases (not shown here).

or with a different superconductor. The dashed line corresponds to $\omega_0/2\pi = 6$ GHz, the value used to investigate the frequency-dependent features of the SIS amplifier. The optimal ac voltage decreases as $\Delta/\hbar\omega_0$ increases (not shown).

For the remainder of this article, we consider an aluminum SIS junction with $\omega_0/2\pi = 6$ GHz ($\Delta/\hbar\omega_0 \approx 7.2$). To further gain insight into the parametric amplifier operational voltages, we investigate the dc- and ac-voltage dependence of single-mode squeezing and phase-preserving gain at zero frequency detuning $\omega' = 0$. Figure 4 shows contours of constant gain (dashed lines) and squeezing (solid lines) in the vicinity of the logarithmic singularity $eV_{\text{dc}} = 2(\Delta - \hbar\omega_0)$.

We first investigate the phase-preserving gain. The different voltage points realizing a given gain do not result in the same device performance, which are characterized by quantum efficiency and 3-dB bandwidth. The former increases when the quasiparticle noise terms in Eq. (16) are reduced. By virtue of the fluctuation-dissipation theorem, noise is related to the dissipation $\text{Re}Y_0$. Figure 4 shows that, in the voltage range of interest, $\text{Re}Y_0$ is nearly independent of dc voltage and increases with increasing ac voltage. Accordingly, along a contour of constant gain, going to lower ac voltage increases the quantum efficiency. Remarkably, we find numerically that it also increases the 3-dB bandwidth. In principle, in the limit $V_{\text{ac}} \rightarrow 0^+$, one would get perfect quantum efficiency, $\xi = 1$. However, for a given gain, decreasing the ac voltage requires the dc voltage to be set increasingly closer to the logarithmic

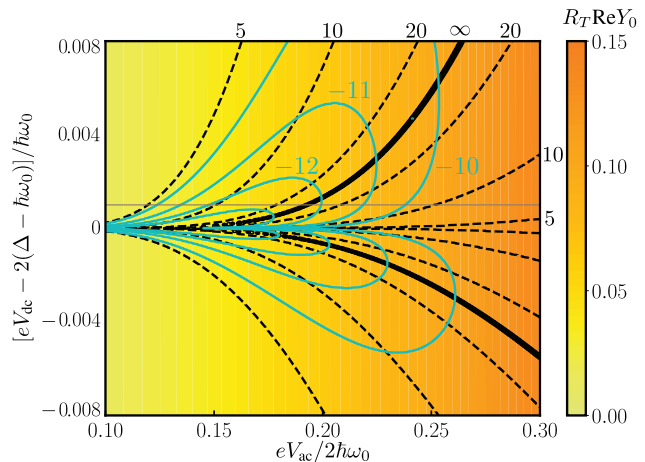


FIG. 4. Dc- and ac-voltage response of an aluminum SIS junction with $\omega_0/2\pi = 6$ GHz ($\Delta/\hbar\omega_0 \approx 7.2$) and $\omega' = 0$: single-photon dissipation $\text{Re}Y_0$ (heat map), phase-preserving gain (dashed contours), and squeezing (solid contours) near the logarithmic singularity $eV_{\text{dc}} = 2(\Delta - \hbar\omega_0)$. Gains from 5 to 20 dB and squeezing between -10 and -13 dB are represented by, respectively, constant values indicated in decibels next to the contours. The thick-solid line indicates voltages where the phase-preserving gain becomes extremely large.

singularity. At some point, the logarithmic singularity is smoothed out by experimental noise on the dc voltage or nonideal I - V curve (finite Dynes parameter). This will set the best experimental performance of the device. For the remainder of the paper, the dc voltage is set to the experimentally relevant value $eV_{dc} = 2\Delta - 1.999\hbar\omega_0$ and, consequently, gain and squeezing are tuned *in situ* by our varying the ac voltage V_{ac} (horizontal line in Fig. 4).

We now turn to squeezing. Similarly to quantum efficiency, squeezing is strongly sensitive to the quasiparticle noise terms, which are related to $\text{Re}Y_0$. For a given V_{ac} , $\text{Re}Y_0$ is almost constant. As a consequence, we expect squeezing to be maximum for the dc voltage giving infinite gain (thick-solid curve in Fig. 4, where the denominator of the gain, $G(\omega) = |r(\omega)|^2$, tends to zero; that is, $|Y_1(-\omega_0)| = |Z_0^{-1} + Y_0(\omega_0) - iC\omega_0|$). At infinite gain, an ideal amplifier would also produce infinite squeezing; however, the finite quasiparticle noise ($\text{Re}Y_0$) bounds squeezing. Analogously to quantum efficiency, maximum squeezing will thus continuously increase by lowering of the ac voltage at the expense of setting the dc voltage closer to the logarithmic discontinuity. Also infinite squeezing could be achieved in the limit $V_{ac} \rightarrow 0^+$, and the maximum experimentally achievable value will be bounded by the smoothing of the logarithmic singularity. Squeezing reaching -15 dB could be achieved with the current experimental setups.

Figure 5 shows phase-preserving gain, quantum efficiency, and squeezing as a function of frequency detuning for $eV_{dc} = 2\Delta - 1.999\hbar\omega_0$ and several ac-voltage amplitudes: $\rho = eV_{ac}/2\hbar\omega_0 \approx 0.151, 0.168, 0.178, 0.184$, and 0.188 . The gain, Fig. 5(a), is observed to increase with increasing ac-voltage amplitude, while its 3-dB bandwidth decreases. In the 20–30-dB range, the gain-bandwidth product is approximately constant, equal to 12 GHz. This value is 87% larger than the gain-bandwidth product of the broadband-impedance-engineered JPA [27]. Figure 5(b) shows that the quantum efficiency is close to 0.9 in the 3-dB-bandwidth frequency range and nearly independent of ac-voltage amplitude. This is expected from the small but finite $\text{Re}Y_0$ observed in Fig. 4. Figure 5(c) illustrates a far-separated two-mode squeezing with 3-dB bandwidth reaching approximately 5.3 GHz. Moreover, unlike gain, squeezing varies only weakly with the ac-voltage amplitude and, after it reaches its maximum value, further increase of the ac-voltage amplitude reduces squeezing, as expected from Fig. 4.

B. Effects of low-frequency noise

The results presented in the previous section are obtained for an ideal SIS junction in the low-temperature limit $k_B T \ll 2\Delta$, for which the transport response is singular and discontinuous for $eV_{dc} = 2\Delta - n\hbar\omega_0$ [51].

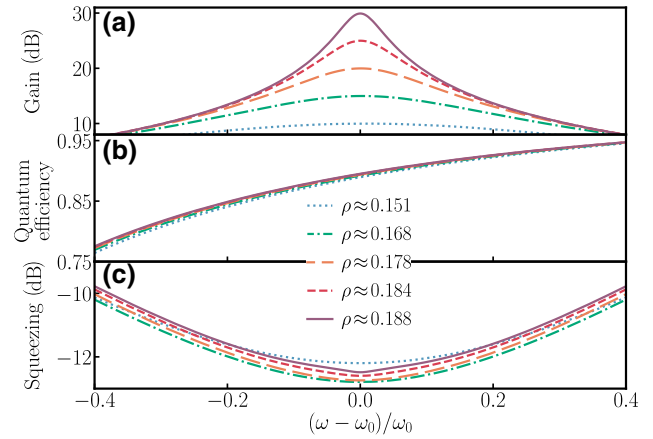


FIG. 5. Aluminum SIS junction with $\omega_0/2\pi = 6$ GHz ($\Delta/\hbar\omega_0 \approx 7.2$): phase-preserving gain (a), quantum efficiency (b), and squeezing (c) as a function of the frequency detuning from ω_0 for the dc voltage $eV_{dc} = 2\Delta - 1.999\hbar\omega_0$ and five different ac-voltage amplitudes, $\rho = eV_{ac}/2\hbar\omega_0 \approx 0.151$ (dotted line), $\rho \approx 0.168$ (dashed-dotted line), $\rho \approx 0.178$ (long-dashed line), $\rho \approx 0.184$ (dashed line), and $\rho \approx 0.188$ (solid line). These values of the ac voltage are chosen such that the phase-preserving gain is, respectively, equal to 10, 15, 20, 25, and 30 dB at zero frequency detuning $\omega = 0$.

However, this is an idealized situation and, in practice, temperature or low-frequency noise can smooth the transport response. Here we consider the effects of low-frequency noise on gain and squeezing properties of the SIS amplifier. These effects are included by assuming that the junction interacts with a low-frequency electromagnetic environment [52] and that the transport properties are described by the $P(E)$ theory [46]. This approach has been shown to quantitatively explain the finite Dynes tunneling density of states [48], usually observed below the dc-transport gap in a normal-insulator-superconductor junction and the corresponding smoothing of the BCS coherence peak [51]. In this approach, the low-frequency noise modifies the equilibrium current noise to

$$S_{eq}^{\text{eff}}(\omega) = \int_{-\infty}^{\infty} S_{eq}(\hbar\omega - E)P(E)dE, \quad (17)$$

where $P(E)$ is the probability density of a tunneling quasiparticle emitting energy E [46].

To model the low-frequency electromagnetic environment, we consider that it originates from the dc-bias scheme. In general, the biasing scheme consists of a resistive voltage divider followed by large capacitive filtering [52,53]. In this situation, the low-frequency impedance is thus the parallel combination of a resistance with a large capacitance C_{br} . This filtering scheme reduces the bandwidth over which low-frequency voltage noise is detrimental to the kilohertz range [53], making the low-frequency voltage fluctuations fully classical. In this setup,

the effect of a low-frequency environment on the transport properties is described by

$$P(E) = \frac{1}{\sqrt{4\pi E_c k_B T}} \exp\left(-\frac{(E - E_c)^2}{4E_c k_B T}\right), \quad (18)$$

where $E_c = e^2/2C_{bt}$ is the capacitor charging energy. With this model, the theory developed in Sec. II remains the same except for the replacement of $S_{eq}(\omega)$ by $S_{eq}^{eff}(\omega)$ in Eq. (12).

Figure 6 illustrates the effect of a low-frequency environment on gain (dashed lines), squeezing (solid lines), and single-photon dissipation ReY_0 (heat map) as a function of dc- and ac voltages. The filtering scheme is characterized by $C_{bt} = 0.1$ nF, corresponding to rms voltage fluctuations of $\sqrt{k_B T/2C_{bt}} \sim 35$ nV. As expected, the low-frequency noise removes the logarithmic singularity at $eV_{dc} = 2(\Delta - \hbar\omega_0)$ (see Fig. 4). Similarly to the ideal case, single-photon dissipation ReY_0 is nearly independent of the dc voltage and increases with increasing ac voltage. Maximization of the device performance will thus again require lowering of the ac voltage. However, along a contour of constant gain (dashed lines) or squeezing (solid lines), V_{ac} now has a finite lower bound. Unlike Fig. 4, where the device performance constantly

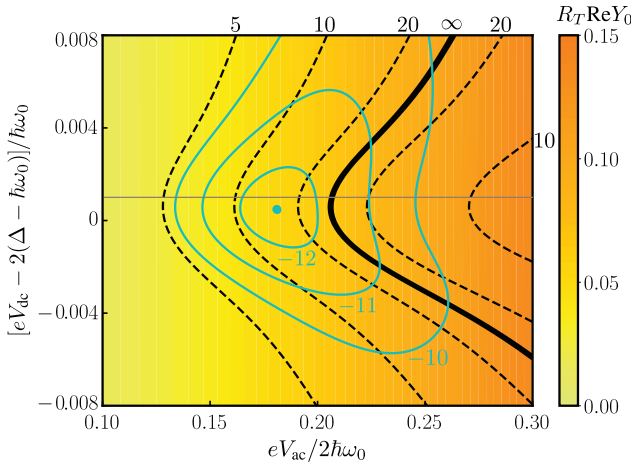


FIG. 6. Dc- and ac-voltage response of an aluminum SIS junction with $\omega_0/2\pi = 6$ GHz ($\Delta/\hbar\omega_0 \approx 7.2$) and $\omega' = 0$: single-photon dissipation ReY_0 (heat map), phase-preserving gain (dashed contours), and squeezing (solid contours) near the logarithmic singularity $eV_{dc} = 2(\Delta - \hbar\omega_0)$ in the presence of a low-frequency environment. The low-frequency-noise filtering scheme is characterized by the capacitor $C_{bt} = 100$ pF, which results in rms voltage fluctuations of 35 nV for $T = 15$ mK. Gains from 5 to 20 dB and squeezing between -10 and -12 dB are represented by, respectively, constant values indicated in decibels next to the contours. The round-blue dot indicates the maximum-squeezing, approximately -12.3 dB, voltage point. The thick solid line indicates voltages where the phase-preserving gain becomes extremely large. The horizontal solid line marks the dc voltage $eV_{dc} = 2\Delta - 1.999\hbar\omega_0$.

increased toward $\xi = 1$ and infinite squeezing by setting the dc voltage closer and closer to the logarithmic singularity $eV_{dc} = 2(\Delta - \hbar\omega_0)$, here we expect approximately constant performance when $2(\Delta - \hbar\omega_0) \lesssim eV_{dc} \lesssim 2\Delta - 1.999\hbar\omega_0$. The presence of low-frequency noise bounds the squeezing to a maximum value of approximately -12.3 dB (round-blue dot). The maximum squeezing depends strongly on the filtering capacitor C_{bt} and it decreases for smaller capacitances. In contrast, the gain remains tunable to any value up to infinity by the dc and ac voltages at the expense of increasing single-photon dissipation ReY_0 .

We now investigate the effects of the low-frequency noise on the frequency-dependent properties of the amplifier. Figure 7 illustrates the gain, quantum efficiency, and squeezing for $eV_{dc} = 2\Delta - 1.999\hbar\omega_0$ and three different filtering capacitances: $C_{bt} \sim 1$ nF, $C_{bt} \sim 0.1$ nF, and $C_{bt} \sim 10$ pF. The ac voltage is set to give 20 dB of gain at zero detuning. These results are compared with the ideal case (solid line), where the junction does not interact with the low-frequency environment. For an aluminum junction ($\Delta/\hbar\omega_0 \approx 10.9$) and $T = 15$ mK, $C_{bt} \sim 1$ nF corresponds to rms voltage fluctuations of $\sqrt{k_B T/2C_{bt}} \sim 11$ nV (dotted line), and the gain, added noise, and squeezing are only weakly affected by the low-frequency environment,

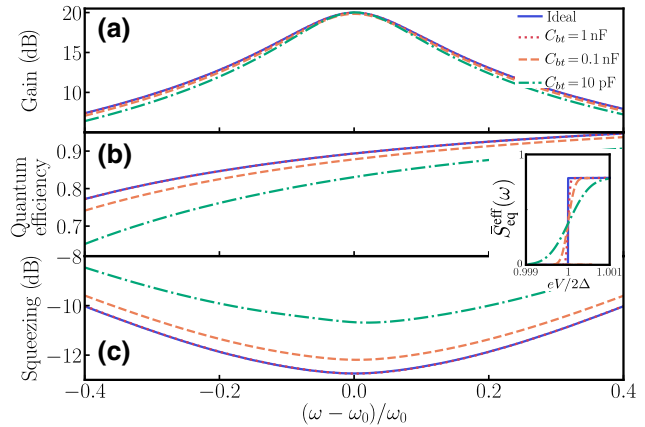


FIG. 7. Aluminum junction ($\Delta/\hbar\omega_0 \approx 10.9$): gain (a), added photon number (b), and squeezing (c) as a function of frequency detuning in the presence and in the absence (solid line) of a low-frequency electromagnetic environment. The dotted line illustrates an efficient ($C_{bt} \sim 1$ nF) filtering scheme. On the other hand, the dashed line ($C_{bt} \sim 0.1$ nF) and the dash-dotted line ($C_{bt} \sim 10$ pF) represent a less-efficient low-frequency-noise filtering. The voltages are chosen such that the gain at zero detuning is equal to 20 dB for all filtering capacitances. As expected, an efficient filtering scheme leads to gain, added noise, and squeezing similarly to the ideal case. Moreover, the gain bandwidth is only weakly affected by the low-frequency electromagnetic environment. However, the amplitude of the quantum efficiency and squeezing are diminished by low-frequency noise. The inset illustrates the effect of the low-frequency environment on equilibrium noise $\bar{S}_{eq}^{eff}(\omega)$ in the unit of $2\Delta/R_T$.

which is efficiently filtered. The effect of low-frequency noise on $S_{\text{eq}}^{\text{eff}}(\omega)$ is illustrated in the inset in Fig. 7. For $C_{bt} \sim 1$ nF, $S_{\text{eq}}^{\text{eff}}(\omega)$ is almost indistinguishable from the ideal case (dashed line), a signature that the low-frequency noise is efficiently filtered. On the other hand, under less-efficient filtering, $C_{bt} \sim 10$ pF corresponding to approximately 0.1 μ V rms voltage fluctuations (dashed line) and $C_{bt} \sim 0.1$ nF, the equilibrium current noise rises smoothly and its behavior near $2\Delta/\hbar$ deviates from the ideal case (see the inset). In these cases, low-frequency noise diminishes both quantum efficiency and squeezing [dashed and dashed-dotted lines in Figs. 7(b) and 7(c)]. However, the 3-dB bandwidth is weakly diminished. Furthermore, the main effect of the low-frequency noise is to diminish the strength of the nonlinearity giving rise to parametric interaction, and therefore to obtain higher gains the ac-voltage amplitude must be increased. The increasing of the ac voltage enhances single-photon dissipation $\text{Re } Y_0$ and degrades quantum efficiency and squeezing.

C. Impedance matching

At first sight, the aforementioned gain-bandwidth product of 12 GHz is quite surprising since the energy scale of the SIS parametric amplifier is the superconducting gap voltage (2Δ), which corresponds to frequencies of approximately 90 GHz for aluminum junctions. To understand what is limiting the gain-bandwidth product, we recall that the phase-preserving gain is determined by the reflection coefficient [Eq. (15)], and its frequency dependence is due to $Y_J(\omega)$ and $\Gamma(\omega)$. Figure 8(a) illustrates the frequency dependence of $Y_J(\omega)$ and $\Gamma(\omega)$ for $eV_{\text{dc}} = 2\Delta - 1.999\hbar\omega_0$ and $eV_{\text{ac}}/2\hbar\omega_0 = 0.178$. The parametric conversion term $\Gamma(\omega)$ is real, independently of the voltages, and is fairly flat in a wide band of frequencies. Also, as expected, the dissipation $\text{Re } Y_0$ is negligible for all frequencies. The contribution of the geometrical capacitance depends weakly on frequency. Consequently, the strong frequency dependence of gain originates from the dynamical susceptance $\text{Im } Y_0$.

To develop a matching scheme to increase the gain-bandwidth product, we first note that the frequency dependence of $\text{Im } Y_0(\omega)$ is modeled with reasonable accuracy by a parallel $L_{\text{eff}}C_{\text{eff}}$ tank with the following characteristics: $\omega_0 R_T C_{\text{eff}} = 0.7$ and $R_T/\omega_0 L_{\text{eff}} = 0.25$. The precise values of L_{eff} and C_{eff} depend on V_{dc} and V_{ac} . However, the above approximate values of L_{eff} and C_{eff} are sufficient to match $\text{Im } Y_0$ for a wide range of voltages. Following Ref. [54], the matching scheme consists in adding, between the SIS junction and the TL, a bandpass-filter network (black box). In the bandpass-filter network, depicted in Fig. 8(b), the first capacitance (inductance) C'_1 (L'_1) is reduced (increased) compared with the original filter capacitance C_1 (inductance L_1) to $C'_1 = C_1 - C_{\text{eff}} - C$ ($1/L'_1 = 1/L_1 - 1/L_{\text{eff}}$). In this manner, the effect of $\text{Im } Y_0$ and C is absorbed in the

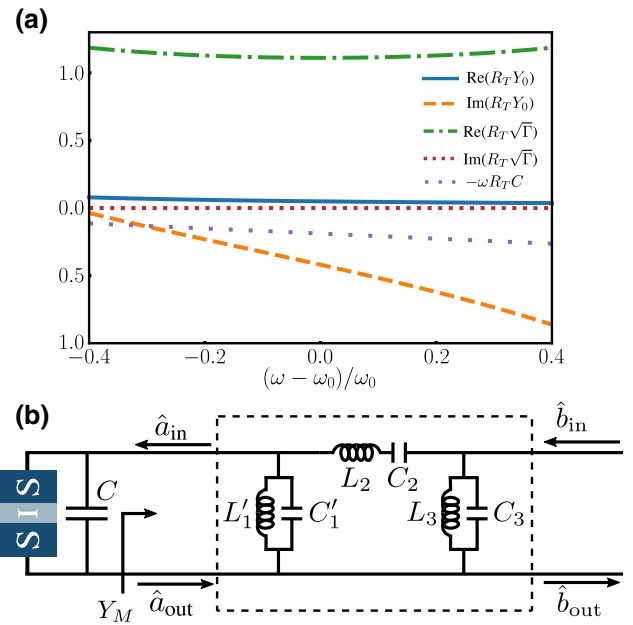


FIG. 8. (a) Frequency dependence of the terms appearing in the reflexion coefficient [Eq. (15)]. Whereas the losses $\text{Re } Y_0$, the parametric two-photon process Γ , and the capacitance ωC are fairly flat, the dynamical susceptance $\text{Im } Y_0$ has a strong frequency dependence. The latter is modeled with reasonable accuracy as a parallel LC tank (i.e., the bandpass-filter structure of the matching network). The parameters used are $\omega_0/2\pi = 6$ GHz, $\Delta/\hbar\omega_0 \approx 7.2$, $eV_{\text{dc}} = 2\Delta - 1.999\hbar\omega_0$, $eV_{\text{ac}}/2\hbar\omega_0 \approx 0.178$, and $C = 100$ fF; they correspond to a phase-preserving gain of 20 dB at frequency $\omega = \omega_0$ in the absence of the matching network. (b) Electrical circuit matching the dynamical susceptance $\text{Im } Y_0$ and geometrical capacitance C of the junction. The input-output operators \hat{a}_{in} and \hat{a}_{out} obey the same equations as those in Fig. 1, in particular Eq. (14). However, the experimentally controllable and measurable observables are the input-output operators \hat{b}_{in} and \hat{b}_{out} . The fields \hat{a} 's and \hat{b} 's are related by the S matrix of the matching network (black box); see Eqs. (19) and (20). The matching network assumes a bandpass-filter structure to compensate the junction dynamical susceptance $\text{Im } Y_0$ and geometrical capacitance C .

filter. Since the filter is designed to achieve good matching in the passband, the detrimental effects of $\text{Im } Y_0$ and C are eliminated.

To obtain an experimentally useful parametric amplifier, we choose filter elements L_n and C_n giving a three-pole Chebyshev filter with 4–8-GHz band edges. Such filters are also characterized by their ripples. While the Chebyshev filter beneficially leads to an increase in the gain-bandwidth product, its ripples impact directly the gain flatness. The ripple amplitude is directly related to the capacitance C_1 of the filter network. To reduce the amplitude of the ripples, the capacitance C_1 must be made as small as possible [54] with the constraint $C'_1 > 0$. In this way, we choose $C_1 \gtrsim C_{\text{eff}} + C$ to minimize the amplitude of the ripples.

Once the elements of the filter are determined, we can readily incorporate it in the quantum formalism via the S -matrix formalism, which gives the sets of linear equations

$$\begin{pmatrix} \hat{b}_{\text{out}}[\omega_0 + \omega'] \\ \hat{a}_{\text{in}}[\omega_0 + \omega'] \end{pmatrix} = S(\omega_0 + \omega') \begin{pmatrix} \hat{b}_{\text{in}}[\omega_0 + \omega'] \\ \hat{a}_{\text{out}}[\omega_0 + \omega'] \end{pmatrix} \quad (19)$$

and

$$\begin{pmatrix} \hat{b}_{\text{out}}^\dagger[\omega_0 - \omega'] \\ \hat{a}_{\text{in}}^\dagger[\omega_0 - \omega'] \end{pmatrix} = S^*(\omega_0 - \omega') \begin{pmatrix} \hat{b}_{\text{in}}^\dagger[\omega_0 - \omega'] \\ \hat{a}_{\text{out}}^\dagger[\omega_0 - \omega'] \end{pmatrix} \quad (20)$$

to be solved together with Eq. (14). Here $S(\omega)$ is the S matrix that connects the SIS-junction fields \hat{a}_{in} and \hat{a}_{out} to the TL fields \hat{b}_{in} and \hat{b}_{out} [see Fig. 8(b)]. With this formalism, the definitions of the gain, quantum efficiency, and squeezing remain the same provided that \hat{a}_{out} is replaced by \hat{b}_{out} . In the presence of the filter, the phase-preserving gain takes the form [55]

$$G(\omega') = \frac{\left| [Y_M^*(\omega_s) - Y_J(\omega_s)] [Y_M^*(\omega_i) + Y_J^*(\omega_i)] + \Gamma(\omega') \right|^2}{\left| [Y_M(\omega_s) + Y_J(\omega_s)] [Y_M^*(\omega_i) + Y_J^*(\omega_i)] - \Gamma(\omega') \right|^2}, \quad (21)$$

where $\omega_s = \omega_0 + \omega'$, $\omega_i = \omega_0 - \omega'$ and Y_M is the filter-matching-network admittance [see Fig. 8(a)].

Figure 9 shows the phase-preserving gain, quantum efficiency, and squeezing for various values of $eV_{\text{ac}}/2\hbar\omega_0$ at $eV_{\text{dc}} = 2\Delta - 1.999\hbar\omega_0$. As shown in Fig. 9(a), the matching scheme dramatically increases the 3-dB bandwidth of the phase-preserving gain to 4.3 GHz, for a gain of 20 dB, from the 1.2-GHz bandwidth obtained without the matching circuit [see Fig. 5(a)]. The gain ripples are induced by the Chebyshev ripples of the filter reflection coefficient; the higher the gain, the higher the amplitude of the ripples. The two extra peaks at the band edges are due to the diminution of $\text{Re}Y_M$ at the band edges, which at some frequency cancel the real part of the denominator of Eq. (21). Reduction of the band-edge peaks can be done by addition of an imaginary part to the denominator of Eq. (21) at the band edges [55]. Here this is achieved by slightly overestimating the first inductance L'_1 .

The compensation of the frequency dependence of $\text{Im}Y_0$ not only increases the 3-dB bandwidth but also enhances the quantum efficiency [Fig. 9(b)] and maximum squeezing [Fig. 9(c)]. The increase of the quantum efficiency and squeezing is due to the reduction of the ac-voltage amplitude and, consequently, single-photon dissipation $\text{Re}Y_0$. For instance, a gain of 20 dB is now achieved with an ac-voltage amplitude of $eV_{\text{ac}}/2\hbar\omega_0 = 0.155$ (dashed-dotted line), a reduction of 13% in comparison with the amplifier without the matching circuit [Fig. 5(a)]. Squeezing now

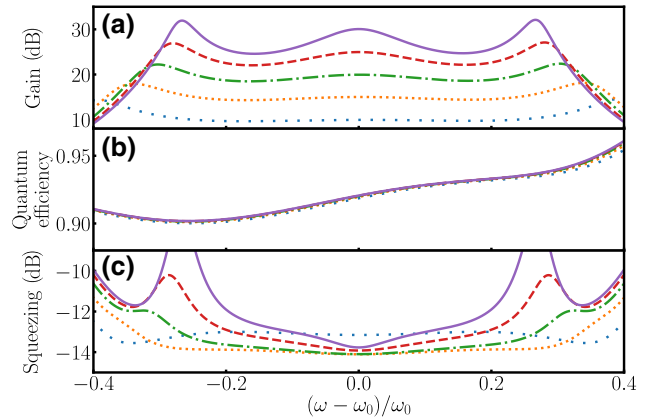


FIG. 9. Matching of an aluminum SIS junction with $\omega_0/2\pi = 6$ GHz ($\Delta/\hbar\omega_0 \approx 7.2$): phase-preserving gain (a), quantum efficiency (b), and squeezing (c) as a function of the frequency detuning from ω_0 for the dc voltage $eV_{\text{dc}} = 2\Delta - 1.999\hbar\omega_0$ and five different ac-voltage amplitudes, $\rho = eV_{\text{ac}}/2\hbar\omega_0 \approx 0.125$ (dotted line), $\rho \approx 0.144$ (long-dotted line), $\rho \approx 0.155$ (dashed-dotted line), $\rho \approx 0.162$ (dashed line), and $\rho \approx 0.166$ (solid line). These values of the ac-voltage amplitude are chosen such that the phase-preserving gain at $\omega = \omega_0$ is equal to 10, 15, 20, 25, and 30 dB, respectively. The values of the matching-circuit parameters are $C'_1 = 0$, $L'_1 \approx 3.39$ nH, $C_2 \approx 424$ fF, $L_2 \approx 1.87$ nH, $C_1 = C_3 \approx 472$ fF, and $L_1 = L_3 \approx 1.68$ nH.

has a complex shape at higher gains but remains extremely flat for $G \leq 15$ dB.

It is remarkable to obtain such an improvement in a wide bandwidth by use of a simple three-pole filter designed to match purely capacitive or inductive elements of passive circuits. Indeed, the SIS parametric amplifier is an active circuit with a nonlinear dynamical susceptibility $\text{Im}Y_0$. Such filters can be fabricated directly on chip either by realization of lumped capacitors and inductors or by use of distributed elements such as $\lambda/4$ lines.

D. Dynamical range

An important characteristic of any parametric amplifier is its dynamical range, which determines how many photons can be amplified without saturating the device. In general, the dynamical range is limited by higher-order nonlinearities of the Hamiltonian and depletion of the pump [56]. Thus, similarly to SIS mixers, we expect the dynamical range for a single-junction amplifier to be small. However, we can ensure that amplification of vacuum fluctuations will not saturate the SIS amplifier. This requires the power of amplified vacuum fluctuations, $P_{\text{vac}} \approx GB\hbar\omega_0$, to be lower than the power delivered by the pump, $P_{\text{pump}} \approx V_{\text{ac}}^2 \text{Re}Y_0(2\omega_0)/2$. However, for amplification in a wide bandwidth, as shown in Fig. 9, we obtain $P_{\text{vac}}/P_{\text{pump}} \approx 1$. This can be overcome by use of a standard approach to design SIS mixers: use of N identical SIS junctions in series. It is shown in Ref. [40] that such an array

is equivalent to a single junction with a pump and saturation power N^2 times larger. The underlying mechanism is easily understood: the impedance of a series array of N SIS junctions is simply N times the impedance of a single junction. Thus, on addition of N junctions of resistance R_T/N in series, the admittance remains the same. However, as the photon-assisted effects, necessary for parametric amplification and squeezing, are proportional to $eV_{\text{ac}}/2\hbar\omega_0$, where V_{ac} is the pump voltage applied to each junction, the *total* pump voltage across the array has to be N times larger. As a consequence, we expect an array of only five to ten SIS junctions to give an experimental relevant dynamical range.

One alternative to increase the dynamical range of a single-junction amplifier is to use a very-low-impedance junction (less than 5Ω), together with an impedance transformer to match the low-impedance junction with the $50-\Omega$ transmission line. Decreasing the junction impedance increases the pump power P_{pump} by the same amount. In practice, a broadband impedance transformation can be implemented either by an extra network of quarter-wavelength transmission lines or directly into the filter matching network by use of shunt resonators and admittance inverters in between [54].

IV. FINAL REMARKS

We propose a near-quantum-limited broadband amplifier and squeezer based on the photon-assisted tunneling of quasiparticles in a SIS junction. This device can function as a phase-sensitive or phase-preserving amplifier. The gain can be tuned by ac-voltage amplitude to obtain gain-bandwidth products of approximately 12 GHz in the 20–30-dB range, which is 87% larger than for the impedance-engineered Josephson parametric amplifier [27]. This device is also a source of far-separated two-mode squeezing with 3-dB bandwidth of approximately 5 GHz and -13 dB of squeezing at the center frequency. Moreover, gain and two-mode squeezing can be fine-tuned *in situ* by our simply changing the pumping-tone amplitude and frequency. For applications with a bandwidth of a few gigahertz, a matching impedance circuit is developed. The proposed matching scheme allows 3-dB bandwidth of 4 GHz. Also, we estimate that the dynamical range of such a broadband amplifier can be enhanced by replacement of the single junction by an array of five to ten SIS junctions. To conclude, the design and fabrication simplicity of this SIS amplifier, together with its operational-mode flexibility, makes it a versatile near-quantum-limited microwave amplifier and squeezer that can be easily integrated in many quantum microwave experiments.

ACKNOWLEDGMENTS

U.C.M. thanks S. Boutin, A.L. Grimsmo, and M. Westig for fruitful discussions, and the Quantronics group

for hospitality. U.C.M., S.J., B.R., and A.B. were supported by the Canada First Research Excellence Fund and NSERC. S.J. and B.R. were supported by Canada Excellence Research Chairs, the Government of Canada, Quebec MEIE, Quebec FRQNT via INTRIQ, Université de Sherbrooke via EPIQ, and the Canada Foundation for Innovation. The research at CEA Saclay received funding from the European Research Council under the European Union's Horizon 2020 program (European Research Council Grant Agreement No. 639039) and support from the ANR AnPhoTeQ research contract.

- [1] A. Wallraff, D. I. Schuster, A. Blais, L. Frunzio, R.-S. Huang, J. Majer, S. Kumar, S. M. Girvin, and R. J. Schoelkopf, Strong coupling of a single photon to a superconducting qubit using circuit quantum electrodynamics, *Nature* **431**, 162 (2004).
- [2] M. A. Castellanos-Beltran and K. W. Lehnert, Widely tunable parametric amplifier based on a superconducting quantum interference device array resonator, *Appl. Phys. Lett.* **91**, 083509 (2007).
- [3] N. Bergeal, F. Schackert, M. Metcalfe, R. Vijay, V. E. Manucharyan, L. Frunzio, D. E. Prober, R. J. Schoelkopf, S. M. Girvin, and M. H. Devoret, Phase-preserving amplification near the quantum limit with a Josephson ring modulator, *Nature* **465**, 64 (2010).
- [4] X. Zhou, V. Schmitt, P. Bertet, D. Vion, W. Wustmann, V. Shumeiko, and D. Esteve, High-gain weakly nonlinear flux-modulated Josephson parametric amplifier using a SQUID array, *Phys. Rev. B* **89**, 214517 (2014).
- [5] C. Eichler, Y. Salathe, J. Mlynek, S. Schmidt, and A. Wallraff, Quantum-Limited Amplification and Entanglement in Coupled Nonlinear Resonators, *Phys. Rev. Lett.* **113**, 110502 (2014).
- [6] S. Jebari, F. Blanchet, A. Grimm, D. Hazra, R. Albert, P. Joyez, D. Vion, D. Esteve, F. Portier, and M. Hofheinz, Near-quantum-limited amplification from inelastic cooper-pair tunnelling, *Nat. Electron.* **1**, 223 (2018).
- [7] T. Walter, P. Kurpiers, S. Gasparinetti, P. Magnard, A. Potocnik, Y. Salathé, M. Pechal, M. Mondal, M. Oppliger, C. Eichler, and A. Wallraff, Rapid High-Fidelity Single-Shot Dispersive Readout of Superconducting Qubits, *Phys. Rev. Appl.* **7**, 054020 (2017).
- [8] R. Vijay, D. H. Slichter, and I. Siddiqi, Observation of Quantum Jumps in a Superconducting Artificial Atom, *Phys. Rev. Lett.* **106**, 110502 (2011).
- [9] Zakka-Bajani Eva, J. Dufouleur, N. Coulombel, P. Roche, D. C. Glattli, and F. Portier, Experimental Determination of the Statistics of Photons Emitted by a Tunnel Junction, *Phys. Rev. Lett.* **104**, 206802 (2010).
- [10] G. Gasse, C. Lupien, and B. Reulet, Observation of Squeezing in the Electron Quantum Shot Noise of a Tunnel Junction, *Phys. Rev. Lett.* **111**, 136601 (2013).
- [11] J. Stehlík, Y.-Y. Liu, C. M. Quintana, C. Eichler, T. R. Hartke, and J. R. Petta, Fast Charge Sensing of a Cavity-Coupled Double Quantum Dot Using a Josephson Parametric Amplifier, *Phys. Rev. Appl.* **4**, 014018 (2015).

- [12] M. Westig, B. Kubala, O. Parlavecchio, Y. Mukharsky, C. Altimiras, P. Joyez, D. Vion, P. Roche, D. Esteve, M. Hofheinz, M. Trif, P. Simon, J. Ankerhold, and F. Portier, Emission of Nonclassical Radiation by Inelastic Cooper Pair Tunneling, *Phys. Rev. Lett.* **119**, 137001 (2017).
- [13] J. O. Simoneau, S. Virally, C. Lupien, and B. Reulet, Photon-pair shot noise in electron shot noise, *Phys. Rev. B* **95**, 060301 (2017).
- [14] A. Bienfait, P. Campagne-Ibarcq, A. H. Kiilerich, X. Zhou, S. Probst, J. J. Pla, T. Schenkel, D. Vion, D. Esteve, J. J. L. Morton, K. Moelmer, and P. Bertet, Magnetic Resonance with Squeezed Microwaves, *Phys. Rev. X* **7**, 041011 (2017).
- [15] B. M. Brubaker *et al.*, First Results from a Microwave Cavity Axion Search at 24 μeV , *Phys. Rev. Lett.* **118**, 061302 (2017).
- [16] M. A. Castellanos-Beltran, K. D. Irwin, G. C. Hilton, L. R. Vale, and K. W. Lehnert, Amplification and squeezing of quantum noise with a tunable Josephson metamaterial, *Nat. Phys.* **4**, 929 (2008).
- [17] K. W. Murch, S. J. Weber, K. M. Beck, E. Ginossar, and I. Siddiqi, Reduction of the radiative decay of atomic coherence in squeezed vacuum, *Nature* **499**, 62 (2013).
- [18] D. M. Toyli, A. W. Eddins, S. Boutin, S. Puri, D. Hover, V. Bolkhovsky, W. D. Oliver, A. Blais, and I. Siddiqi, Resonance Fluorescence from an Artificial Atom in Squeezed Vacuum, *Phys. Rev. X* **6**, 031004 (2016).
- [19] N. Didier, A. Kamal, W. D. Oliver, A. Blais, and A. A. Clerk, Heisenberg-Limited Qubit Read-Out with Two-Mode Squeezed Light, *Phys. Rev. Lett.* **115**, 093604 (2015).
- [20] S. Puri and A. Blais, High-Fidelity Resonator-Induced Phase Gate with Single-Mode Squeezing, *Phys. Rev. Lett.* **116**, 180501 (2016).
- [21] B. Royer, A. L. Grimsmo, N. Didier, and A. Blais, Fast and high-fidelity entangling gate through parametrically modulated longitudinal coupling, *Quantum* **1**, 11 (2017).
- [22] S. L. Braunstein and P. van Loock, Quantum information with continuous variables, *Rev. Mod. Phys.* **77**, 513 (2005).
- [23] A. L. Grimsmo and A. Blais, Squeezing and quantum state engineering with Josephson travelling wave amplifiers, *npj Quantum Inf.* **3**, 20 (2017).
- [24] S. Boutin, D. M. Toyli, A. V. Venkatramani, A. W. Eddins, I. Siddiqi, and A. Blais, Effect of Higher-Order Nonlinearities on Amplification and Squeezing in Josephson Parametric Amplifiers, *Phys. Rev. Appl.* **8**, 054030 (2017).
- [25] M. P. Westig and T. M. Klapwijk, Josephson Parametric Reflection Amplifier with Integrated Directionality, *Phys. Rev. Appl.* **9**, 064010 (2018).
- [26] J. Y. Mutus, T. C. White, R. Barends, Y. Chen, Z. Chen, B. Chiaro, A. Dunsworth, E. Jeffrey, J. Kelly, A. Megrant, C. Neill, P. J. J. O’Malley, P. Roushan, D. Sank, A. Vainsencher, J. Wenner, K. M. Sundqvist, A. N. Cleland, and J. M. Martinis, Strong environmental coupling in a Josephson parametric amplifier, *Appl. Phys. Lett.* **104**, 263513 (2014).
- [27] T. Roy, S. Kundu, M. Chand, A. M. Vadiraj, A. Ranadive, N. Nehra, M. P. Patankar, J. Aumentado, A. A. Clerk, and R. Vijay, Broadband parametric amplification with impedance engineering: Beyond the gain-bandwidth product, *Appl. Phys. Lett.* **107**, 262601 (2015).
- [28] C. Macklin, K. O’Brien, D. Hover, M. E. Schwartz, V. Bolkhovsky, X. Zhang, W. D. Oliver, and I. Siddiqi, A near-quantum-limited Josephson traveling-wave parametric amplifier, *Science* **350**, 307 (2015).
- [29] C. W. J. Beenakker and H. Schomerus, Antibunched Photons Emitted by a Quantum Point Contact out of Equilibrium, *Phys. Rev. Lett.* **93**, 096801 (2004).
- [30] A. D. Armour, M. P. Blencowe, E. Brahimi, and A. J. Rimberg, Universal Quantum Fluctuations of a Cavity Mode Driven by a Josephson Junction, *Phys. Rev. Lett.* **111**, 247001 (2013).
- [31] Juha Leppäkangas, Mikael Fogelström, Alexander Grimm, Max Hofheinz, Michael Marthaler, and Göran Johansson, Antibunched Photons from Inelastic Cooper-Pair Tunneling, *Phys. Rev. Lett.* **115**, 027004 (2015).
- [32] U. C. Mendes and C. Mora, Cavity squeezing by a quantum conductor, *New J. Phys.* **17**, 113014 (2015).
- [33] U. C. Mendes and C. Mora, Electron-photon interaction in a quantum point contact coupled to a microwave resonator, *Phys. Rev. B* **93**, 235450 (2016).
- [34] J. Zmuidzinas and P. L. Richards, Superconducting detectors and mixers for millimeter and submillimeter astrophysics, *Proc. IEEE* **92**, 1597 (2004).
- [35] M. P. Westig, K. Jacobs, J. Stutzki, M. Schultz, M. Justen, and C. E. Honingh, Balanced superconductor-insulator-superconductor mixer on a 9 μm silicon membrane, *Supercond. Sci. Technol.* **24**, 085012 (2011).
- [36] G. S. Lee, Superconductor-Insulator-Superconductor Reflection Parametric Amplifier, *Appl. Phys. Lett.* **41**, 291 (1982).
- [37] I. A. Devyatov, L. S. Kuzmin, K. K. Likharev, V. V. Migulin, and A. B. Zorin, Quantum-statistical theory of microwave detection using superconducting tunnel junctions, *J. Appl. Phys.* **60**, 1808 (1986).
- [38] Yurke Bernard and S. Denker John, Quantum network theory, *Phys. Rev. A* **29**, 1419 (1984).
- [39] P. K. Tien and J. P. Gordon, Multiphoton process observed in the interaction of microwave fields with the tunneling between superconductor films, *Phys. Rev.* **129**, 647 (1963).
- [40] J. R. Tucker and M. J. Feldman, Quantum detection at millimeter wavelengths, *Rev. Mod. Phys.* **57**, 1055 (1985).
- [41] C. W. Gardiner and M. J. Collett, Input and output in damped quantum systems: Quantum stochastic differential equations and the master equation, *Phys. Rev. A* **31**, 3761 (1985).
- [42] M. H. Devoret, D. Esteve, H. Grabert, G.-L. Ingold, H. Pothier, and C. Urbina, Effect of the Electromagnetic Environment on the Coulomb Blockade in Ultrasmall Tunnel Junctions, *Phys. Rev. Lett.* **64**, 1824 (1990).
- [43] A. L. Grimsmo, F. Qassemi, B. Reulet, and A. Blais, Quantum Optics Theory of Electronic Noise in Coherent Conductors, *Phys. Rev. Lett.* **116**, 043602 (2016).
- [44] C. Mora, C. Altimiras, P. Joyez, and F. Portier, Quantum properties of the radiation emitted by a conductor in the Coulomb blockade regime, *Phys. Rev. B* **95**, 125311 (2017).

- [45] Fourier transform of the operator $\hat{I}[t]$ is defined as $\hat{I}[\omega] = \int_{-\infty}^{\infty} \hat{I}(t)e^{i\omega t} dt$, in accordance with the quantum-mechanics definition.
- [46] G.-L. Ingold and Yu. V. Nazarov, Single Charge Tunneling, edited by H. Grabert and M. H. Devoret (Plenum Press, New York, 1992).
- [47] A. A. Clerk, M. H. Devoret, S. M. Girvin, F. Marquardt, and R. J. Schoelkopf, Introduction to quantum noise, measurement, and amplification, *Rev. Mod. Phys.* **82**, 1155 (2010).
- [48] J. P. Pekola, V. F. Maisi, S. Kafanov, N. Chekurov, A. Kemppinen, Yu. A. Pashkin, O.-P. Saira, M. Möttönen, and J. S. Tsai, Environment-Assisted Tunneling as an Origin of the Dynes Density of States, *Phys. Rev. Lett.* **105**, 026803 (2010).
- [49] C. M. Caves, Quantum limit on noise in linear amplifiers, *Phys. Rev. D* **26**, 1817 (1982).
- [50] P. N. Chubov, V. V. Eremenko, and Yu. A. Pilipenko, Dependence of the critical temperature and energy gap on the thickness of superconducting aluminum films, Sov. Phys. JETP **28**, 389 (1969).
- [51] A. Barone and G. Paterno, *Physics and Applications of the Josephson Effect* (Wiley-Interscience, New York, NY, 1982).
- [52] M. Hofheinz, F. Portier, Q. Baudouin, P. Joyez, D. Vion, P. Bertet, P. Roche, and D. Esteve, Bright Side of the Coulomb Blockade, *Phys. Rev. Lett.* **106**, 217005 (2011).
- [53] F. Chen, J. Li, A. D. Armour, E. Brahimi, J. Stettenheim, A. J. Sirois, R. W. Simmonds, M. P. Blencowe, and A. J. Rimberg, Realization of a single-cooper-pair Josephson laser, *Phys. Rev. B* **90**, 020506 (2014).
- [54] G. L. Matthaei, L. Young, and E. M. T. Jones, *Microwave Filters, Impedance-Matching Networks, and Coupling Structures* (McGraw-Hill Book Company, Norwood, MA, 1964).
- [55] G. L. Matthaei, A study of the optimum design of wide-band parametric amplifiers and up-converters, *IRE Trans. Microwave Theory Tech.* **9**, 23 (1961).
- [56] Ananda Roy and Michel Devoret, Quantum-limited parametric amplification with Josephson circuits in the regime of pump depletion, *Phys. Rev. B* **98**, 045405 (2018).